PERGAMON

International Journal of Heat and Mass Transfer 41 (1998) 3691–3704

International Journal of HEAT and MASS TRANSFER

Experimental study of critical heat flux in concentric-tube open thermosyphon

Md. Ashraful Islam, Masanori Monde*, Mohammad Z. Hasan, Yuichi Mitsutake

Department of Mechanical Engineering, Saga University, 1 Honjo-machi, Saga-shi, Saga 840, Japan

Received 22 September 1997; in final form 9 April 1998

Abstract

An experimental study has been performed to understand the critical heat flux (CHF) mechanism in an open concentric-tube thermosyphon by which the CHF can be increased by several times compared to a conventional one. Experiments are conducted with saturated water, R113, and ethanol at various working pressures and by varying different geometrical parameters of the thermosyphon such as inner diameter of the outer tube, outer diameter of the inner tube, and heated length. For a particular heated tube diameter working with a specific fluid, there is an optimum diameter of the inner tube for which the CHF is maximum. The optimum diameter of the inner tube divides the CHF into two characteristic regions. The CHF characteristics in each region are discussed and then correlations for predicting the CHF data are proposed.

Nomenclature

C constant
D_{he} equivalent heated diameter, [mm] = (4 × flow area)/(heated perimeter) = $(D_i^2 - d_o^2)/D_i$, for outer tube heated
D_i inner diameter of the heated tube [mm]
d_i inner diameter of the inner unheated tube [mm]
d_o outer diameter of the inner unheated tube [mm]
g gravitational acceleration [m s^{-2}]
H_{fg} latent heat of evaporation [kJ kg^{-1}]
Ku Kutateladze number = $q_{co}/(\rho_v H_{fg})/^4\sqrt{\sigma(\rho_l - \rho_v)g/\rho_v^2}$
L heated tube length [mm]
P system pressure [MPa]
q heat flux [MW m^{-2}]
q_{co} CHF for saturated boiling [MW m^{-2}]
$q_{co,0}$ q_{co} without inner tube [MW m^{-2}]
s annular gap, $(D_i - d_o)/2$ [mm]
T_w heated wall temperature [°C]
T_{sat} saturation temperature [°C]
ΔT_{sat} wall superheat, $(T_w - T_{sat})$ [K].

Greek symbols
Φ^* $= (4L/D_i)Ku/0.16(\rho_l/\rho_v)^{0.13}$
ρ density [kg m^{-3}]
σ surface tension [N m^{-1}].

Subscripts
he heated equivalent
i inner
l liquid
o outer
sat saturation
v vapor
w wall.

1. Introduction

A two-phase thermosyphon, a device that utilizes buoyancy force and phase change of liquid contained in a vertical tube for heat transfer without the aid of an external work, has been studied extensively for many years for different geometric configurations in order to investigate the heat transfer characteristics and the operating limits. There are many actual and suggested applications of two-phase thermosyphon for taking advantage

*Corresponding author.

0017–9310/98 $19.00
PII: S0017–9310(98)00149–5

of its high effective thermal conductivity. It can be used, for example, for cooling electronic circuits, gas turbine blades, and the plasma facing components in fusion reactors, and extracting geothermal energy and preserving permafrost.

Critical heat flux (CHF) in a thermosyphon, beyond which the heat transfer process is largely degraded, is considered as a phenomenon closely related to flooding which is a limiting condition in a countercurrent flow. Hence, the most generalized correlations for the CHF data have depended mainly on flooding [1, 2]. Imura et al. [3] analyzed their own CHF data along with the other existing data to give the following correlation:

$$Ku = 0.16(D_i/L)(\rho_l/\rho_v)^{0.13} \quad (1)$$

where Ku is the Kutateladze number, D_i is the inner diameter of the thermosyphon, L is the heated length of the thermosyphon, and ρ_l and ρ_v are the densities of liquid and vapor, respectively. On the other hand, many analytical studies were performed by Dobran [4], Reed and Tien [5], Lock [6], Katto [7] and others. Most recently, Monde [8] developed an analytical model to evaluate the CHF in the thermosyphon from the maximum falling liquid flow rate and showed that the evaluated CHF is in fairly good agreement with the existing CHF data.

The effective thermal conductivity in a conventional thermosyphon can be significantly improved by inserting a tube concentrically into it. This is attributed to the fact that the inner tube enables liquid to be supplied to the thermosyphon without any interaction with the escaping vapor flow. There have been a few investigations in this regard. Seki et al. [9] investigated convective heat transfer in an open concentric-tube thermosyphon and found that the presence of inner tube markedly increases the overall heat transfer coefficient. In addition to this, Seki et al. [10] conducted experiments on the same thermosyphon in order to investigate boiling heat transfer characteristics of R-11 and prescribed a way of predicting the total heat flux. Fukuda et al. [11] experimented on a double-cylinder closed thermosyphon to collect the data on heating limits and reported that the heating limit is 1.8 times higher than that in a conventional one. A recent study on concentric-tube thermosyphon was carried out by Mitsutake et al. [12]. They have collected the CHF data for limited experimental ranges and reported that the use of inner tube enhances the CHF for an optimum condition as much as six times of that in a conventional one.

From the foregoing survey, it is clear that the CHF characteristics in the concentric-tube thermosyphon need to be investigated for a wide experimental range and that the fundamental design informations need to be provided to apply the system as an efficient heat transfer device.

The purpose of the present study is, therefore, to experimentally investigate the CHF characteristics in a concentric-tube open thermosyphon which is a bottom-closed outer tube with an inner tube inserted concentrically. These experiments are conducted to understand the geometric effects on the CHF enhancement. In particular, different combinations of outer and inner tubes in the concentric-tube thermosyphon have been investigated in order to get the optimum one that provides the maximum CHF. Moreover, an attempt has been made to explain the characteristics of the CHF.

2. Experimental apparatus and procedure

2.1. *Test facility*

The test facility to measure the CHF in the present thermosyphon is shown in Fig. 1. The facility consists of

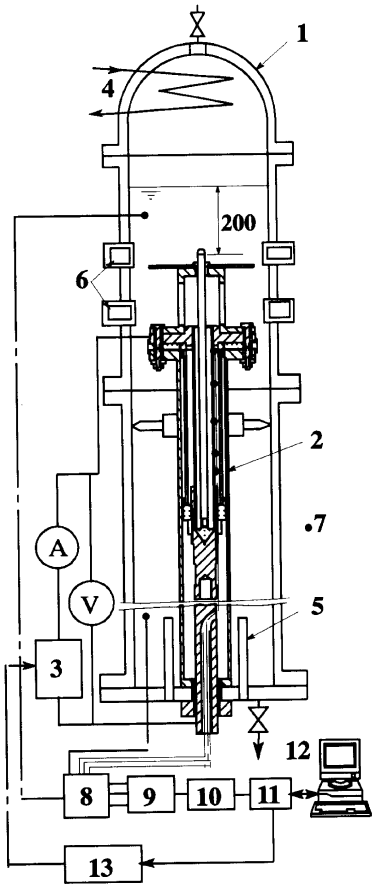

Fig. 1. A schematic of the experimental apparatus where the numbered items are: (1) pressure vessel, (2) thermosyphon assembly, (3) DC power supply, (4) cooling coil, (5) auxiliary heater, (6) windows, (7) thermocouple locations, (8) ice box, (9) multiplexer, (10) digital thermometer, (11) GPIB, (12) computer (13) GPIB programmer.

the pressure vessel, DC power supply, data acquisition, and control system. The pressure vessel, which is about 2170 mm high and 200 mm in diameter, contains the thermosyphon assembly and test fluid. Auxiliary heaters and cooling coils are also placed in the vessel to maintain the system pressure at a designated saturation temperature. Several windows are provided in the vessel for flow observation at the exit of the thermosyphon.

Figure 2 shows a schematic of the thermosyphon assembly. The concentric-tube thermosyphon is the bottom-closed outer tube with a tube inserted concentrically into it. A commercial seamless steel tube of 1 mm wall-thickness is used as the outer tube both ends of which are shrink-fitted into cylindrical brass electrodes and subsequently are silver-soldered to reduce the electrical contact resistance as much as possible and to prevent the leakage of liquid at high pressure. This tube is directly heated by a DC power supply. Several Chromel–Alumel thermocouples are attached on the outer surface of the outer tube at different locations as shown in Fig. 2 to monitor the wall temperatures. The number of thermocouples varies with the length of the heated tube. There are 6, 5, 4, and 3 thermocouples for the heated tube lengths of 1000, 500, 250 and 100 mm respectively. The temperatures at several points are monitored in order to minimize the time lag of CHF detection.

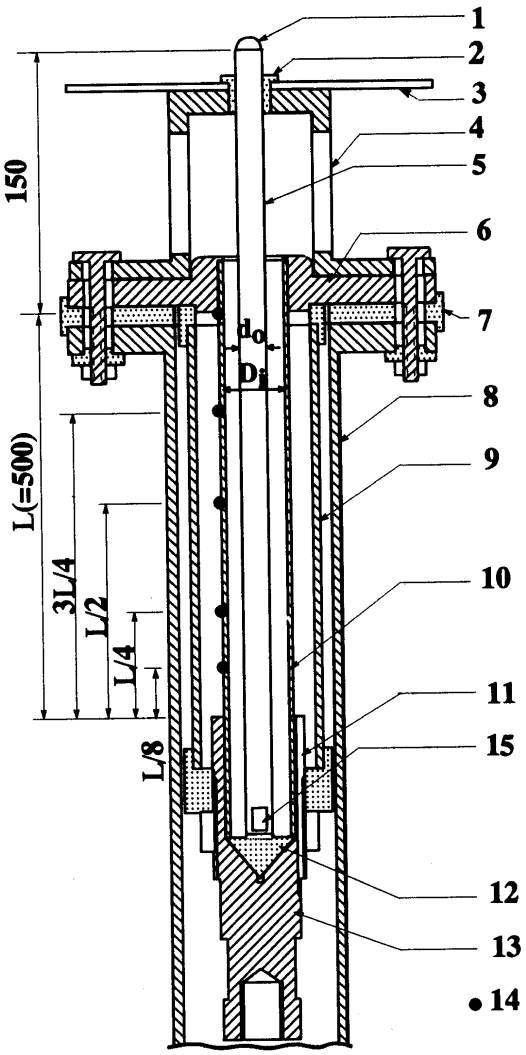

Fig. 2. A schematic of the thermosyphon assembly where the numbered items are: (1) tuft, (2) Bakelite brush, (3) baffle disc, (4) tripoid fixture, (5) inner tube, (6) upper electrode, (7) Bakelite disc, (8) brass pipe, (9) brass jacket, (10) heated tube, (11) slot for thermocouple, (12) conical Bakelite, (13) lower electrode, (14) thermocouple locations, (15) opening.

The inner tube, which is about 150 mm longer than the outer tube, is also a commercial stainless steel tube of 0.5 mm wall-thickness. The longer inner tube is needed to fix it concentrically within the outer tube, to facilitate easy vapor escape and also to overcome the shrink-fitted length of the outer tube. The concentricity of this tube with the outer tube is maintained by a bakelite bush fitted in the fixture at the top and by a conical Bakelite sitting on the conical seat machined in the lower electrode. The usage of bakelite at the top and bottom makes the inner tube electrically insulated from the heated tube. The bottom end of the inner tube provides two openings for liquid to flow through it, and the top end has a tuft to show the flow direction. A baffle disc is attached as shown in Fig. 2 to prevent sucking of vapor into the inner tube. Different combinations of the outer and inner tubes are selected to have annular gaps ranging from 1–6 mm.

A brass jacket is fitted around the thermosyphon to provide a tension in the heated tube in order to compensate for the thermal expansion of the same; however, the bottom end of the thermosyphon is also free to move downward. So, the brass jacket serves as a double check for unwanted bending of the heated tube due to thermal stress. The outermost brass pipe acting as the container of the thermosyphon is so designed that the test liquid can enter from the top only. The still air layer between the brass pipe and the heated tube serves as the thermal insulation.

A 30 V–1000 A rated DC power supply in series with a shunt resistor is connected to the outer tube. The shunt resistor, rated 50 mV–1000 A, is used to determine the current in the electric circuit. The measured voltage drop across the heated tube of the thermosyphon and current are used to calculate the heat input. The maximum axial heat loss from the heated tube is estimated to be less than 1% of the electric input according to one dimensional heat conduction calculation. Again, the radial heat loss is estimated to be much less than 1%. Therefore, heat input to the thermosyphon is equal to the measured electric power with an uncertainty of not more than 2%. Similar estimation errors were also reported in the previous studies, [13] and [14].

The data acquisition system comprising of BASIC code, GP-IB and its programmer, and digital multi-thermometer records the heated well temperature, liquid temperature, voltage drop across the heated tube and current passing through it.

2.2. *Test procedure*

The pressure vessel is first filled with the test liquid up to 200 mm above the top of the inner tube. This extra liquid head stabilizes the system pressure at any prescribed magnitude. The liquid is heated up to the saturated temperature at a designated pressure by auxiliary heaters and is maintained in this condition by thermostatically adjusting the power of the heaters and by regulating the water flow rate in the cooling circuit. After the steady state condition is confirmed (liquid temperature change within ± 0.5 K), heat is added to the thermosyphon tube in steps from the DC power supply. After each heat flux increment, instantaneous wall-temperatures of the heated tube are monitored and then each measurement is taken after the steady state condition is confirmed within 50 s. Within this period, after every 5 s, the instantaneous wall-temperatures are compared with the temperature of the liquid bath. The wall-temperature, at a certain heat flux and location, starts running away or increasing monotonically and then the CHF is defined to have occurred. After the CHF is detected, the power supply is automatically cut off when the difference between the wall and saturation temperatures exceeds 80 K. Near the CHF, the voltage increment is not more than 1% of the preceding voltage step, which ensures the total uncertainty in the CHF data to be estimated within 3%. Three consecutive runs are conducted for each set of experimental conditions and the data reproducibility is confirmed within 3%.

3. Results and discussion

Two hundred and forty-one CHF data are collected for the present thermosyphon by varying different parameters listed in Table 1. The wall temperatures of the outer tube have also been recorded in order to get the boiling curve and the CHF location as well. The flow condition at the exit of the thermosyphon is observed to have some information regarding the CHF mechanism. Before discussing the effects of inner tube on the CHF and the characteristics of the CHF, the flow condition, boiling curves and the CHF locations are discussed sequentially.

3.1. *Flow observation*

At a certain wall superheat, bubbles are formed at favorable sites on the heated tube wall and move upward due to the buoyancy effect with subsequent suction of liquid into the inner tube accounting for continuity. At a particular heat flux, liquid flowing through the inner tube changes its flow direction depending upon the dimensions of the thermosyphon. Near the CHF, five different flow patterns can be drawn (Fig. 3) according to the flow observation at the open end of the thermosyphon: (A) vapor jet comes up through the annulus interacting with some liquid entering through it while major portion of liquid is supplied by the inner tube; (B) isolated vapor bubbles flow up through the inner tube, whereas vapor jet escapes through the annulus and most of liquid has been supplied by the inner tube as in (A); (C) sucking flow through the inner tube with subsequent vapor flow

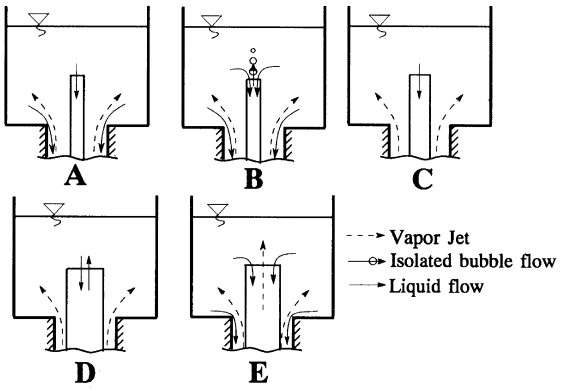

Fig. 3. A schematic of the flow pattern near the open end of the thermosyphon.

Table 1. Experimental ranges

Fluid	Water	R113	Ethanol [12]
P [MPa]	0.1	0.1, 0.2, 0.3	0.1, 0.2, 0.3
ρ_l/ρ_v	1605.2	202.2, 102.4, 67.6	446.4, 232.7, 106.7
D_i (d_o) [mm(mm)]	17 (0, 5, 9, 13, 15), 12 (0, 4, 6, 8, 10), 9 (0, 3, 5, 7) and 5 (0, 3)	17 (0, 5, 9, 13, 15), 12 (0, 4, 6, 8, 10), 9 (0, 3, 5, 7) and 5 (0, 3)	17 (0, 5, 9, 13, 15)
L [mm]	100, 250, 500, 1000	100, 250, 500, 1000	1000, 500

through the annulus; (D) oscillating flow where liquid flow in the inner tube is found oscillating between upward and downward and the vapor jet flows up along the annulus; and (E) reverse flow where vapor jet comes up from the inner tube and vapor like a coalesced bubble comes out from the annulus through which most of liquid has been supplied.

The relationship between flow pattern and geometric dimensions of concentric-tube thermosyphons for $D_i = 12$ mm is also given as an example in Table 2 for both water and R113. The relationship for other combinations of inner and outer tube diameters is omitted here because the similar relationship was found. The flow patterns of types A, B, C, and E are observed for water, whereas for R113 the types of flow patterns are of A, C, and D. For ethanol [12], the flow patterns are reported similar to R113 in the narrow experimental ranges given in Table 1. The differences in flow pattern for different test fluid seems to be attributed to the density ratio and the characteristic length scale of each fluid (Laplace number).

3.2. *Boiling curve*

Boiling in a vertical annulus heated from outside is more complicated than that of common boiling in a pool, because the vapor-bubbles cannot rise freely from a submerged heater but are constrained to rise in a relatively narrow space, becoming more and more crowded and displacing more liquid. Boiling curves for the present concentric-tube thermosyphon are drawn to understand the boiling process.

Figure 4 shows the heat transfer rate q as a function of the wall superheat ΔT_{sat} for the thermosyphon, 1000 mm in length and 12 mm in diameter, working with water for different inner tubes. Each symbol represents a representative boiling curve at the point on the heated tube where the CHF is detected for a particular inner tube. Boiling curves for the other measuring points have the same trend up to the CHF and are omitted here for clarity. Figure 4 also shows the Rohsenow correlation [15] for pool boiling, the Imura et al. prediction [16] for conventional thermosyphon, and the Seki et al. correlation [10] for concentric-tube open thermosyphon.

Table 2. Flow patterns of thermosyphons of $D_i = 12$ mm working with water and R113

	L [mm]			
d_o [mm]	1000	500	250	100
4	B (A)	A (A)	A (A)	A (A)
6	B (C)	C (C)	C (C)	C (C)
8	E (C)	E (C)	E (C)	C (C)
10	E (C)	E (D)	E (D)	E (D)

Letters in parentheses are the flow patterns for R113.

The plot of q vs ΔT_{sat} shows that the characteristic of boiling heat transfer for different inner tubes except the smallest gap of $d_o = 10$ mm seems to be rather similar to the result obtained for pool boiling by Rohsenow [15] and for the conventional thermosyphon by Imura et al. [16], while the Seki et al. correlation [10] behaves differently, the reason for which is not clear. The CHF for $d_o = 4$, 6, and 8 mm are enhanced compared with that for $d_o = 0$ (conventional thermosyphon). On the other hand, for the case of $d_o = 10$ mm, the data in the $q-\Delta T_{sat}$ plot exhibit significantly different trends near the CHF, and the CHF becomes lower than that for $d_o = 0$.

In the region of the boiling curve where the temperature is decreased with an increase in heat flux, the heat transfer is clearly enhanced by evaporation of thin liquid film in which ordinary boiling is suppressed. The phenomenon that the boiling is suppressed due to film evaporation is commonly observed under annular flow pattern in a forced convective flow boiling [17]. It is worth mentioning that this phenomenon is always observed for the cases of $d_o = 0$, 4, 6, and 8 mm just below the CHF point.

The reason why the CHF for $d_o = 10$ mm becomes lower than that for $d_o = 0$ may be that the vapor flow is restricted by the inserted tube because the CHF took place under the flow pattern of the type E in Fig. 3.

3.3. *CHF location*

Figure 5 shows the wall temperature variation of the heated tube of the concentric-tube thermosyphon ($L = 1000$ mm, $D_i = 12$ mm and $d_o = 10$ mm) working with water at atmospheric pressure at the heat flux of 0.0228 MW/m^2 at which the CHF is detected. Here, the time of the temperature variation is the period through which the thermosyphon worked under this heat flux. The origin of the time is taken as that moment at which the wall temperature at a certain location starts increasing monotonically. Each symbol in the figure denotes the thermocouple location from the bottom of the heated tube.

It is found from Fig. 5 that normal operation continues for 13 s after the power is increased to the heat flux of 0.0228 MW/m^2. After 13 s, the wall temperature at the bottom half of the heated tube starts increasing monotonically and the CHF location is detected at $L/8$ after 33 s by the present data acquisition algorithm. Before the CHF location is detected, the wall temperatures at $3L/4$ and $L/16$ start decreasing due to liquid penetration which results from the reduction of net vapor generation after the inception of CHF because a part of heat being supplied to the heated tube is consumed as sensible heat to increase the wall temperature. Liquid penetrates to the

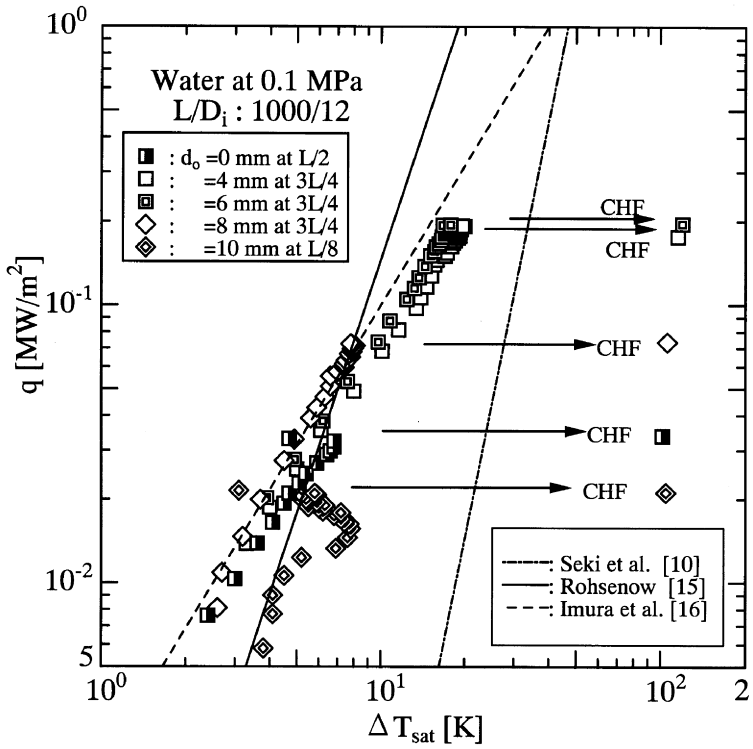

Fig. 4. Boiling curves at the CHF locations.

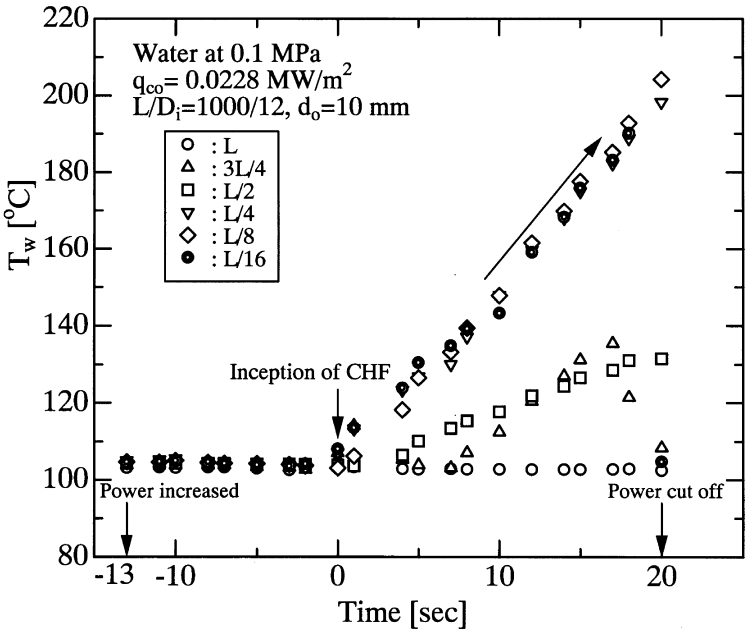

Fig. 5. Wall temperature variation at CHF.

point of $3L/4$ along the tube wall of the annulus, while to the point of $L/16$ through the inner tube.

Without the inner tube, the CHF is found to occur at the lower part (within $L/4$) of the thermosyphon. With the inner tube, the CHF location is found differently according to the working fluid in the present experimental ranges. For R113, the CHF locations are always found near the top of the heated tube, while for water the CHF is found to occur at different locations in the upper half of the heated tube with a few exceptions having annular gap of 1 mm. For the annular gap of 1 mm, the CHF occurs at the lower half of the heated tube because the CHF takes place under the flow pattern of the type E in Fig. 3, as mentioned in section 3.1.

3.4. *CHF in a conventional thermosyphon*

The CHF data for a conventional thermosyphon (having no inner tube) are well predicted by the correlation (1) which can be reduced to the Kutateladze equation with the constant of 0.16 for predicting the CHF in an ordinary saturated pool boiling. In the light of correlation (1), $Ku/0.16(\rho_l/\rho_v)^{0.13}$ is tentatively chosen in place of the CHF of a thermosyphon working with a particular liquid at a specific pressure. Figure 6 shows the variation of $Ku/0.16(\rho_l/\rho_v)^{0.13}$ with the length/diameter ratio (L/D_i) of the present thermosyphon without inner tube. Here, the thick line is the fitted values of the analytical prediction by Monde [8] and the dashed line is the Imura et al. correlation (1).

Figure 6 shows that the CHF data are in good agreement with correlation (1) and the Monde [8] prediction. The Monde model always predicts the CHF higher than that predicted by correlation (1). In [8], the maximum falling liquid flow rate into the tube during a countercurrent flow is adopted.

3.5. *Effects of inner tube on CHF*

Figure 7 shows typical variation of the CHF for water and R113 with the inner tube diameter at a fixed outer tube diameter of $D_i = 12$ mm. The CHF increases up to a certain diameter of the inner tube and then decreases continuously as the inner tube diameter approaches the outer tube diameter. Therefore, the diameter of the inner tube at which the CHF is maximum is called the optimum diameter. Figure 7 clearly shows the existence of optimum diameter. The present selection of the inner tube diameters is not wide enough to accurately specify the optimum diameter. Within the present experimental ranges, the outer tube diameter has significant effects on the optimum diameter but the length of the outer tube seems to have a weak effect. The larger diameter of the outer tube makes the optimum inner tube diameter larger. The working fluid may have some effects on the optimum

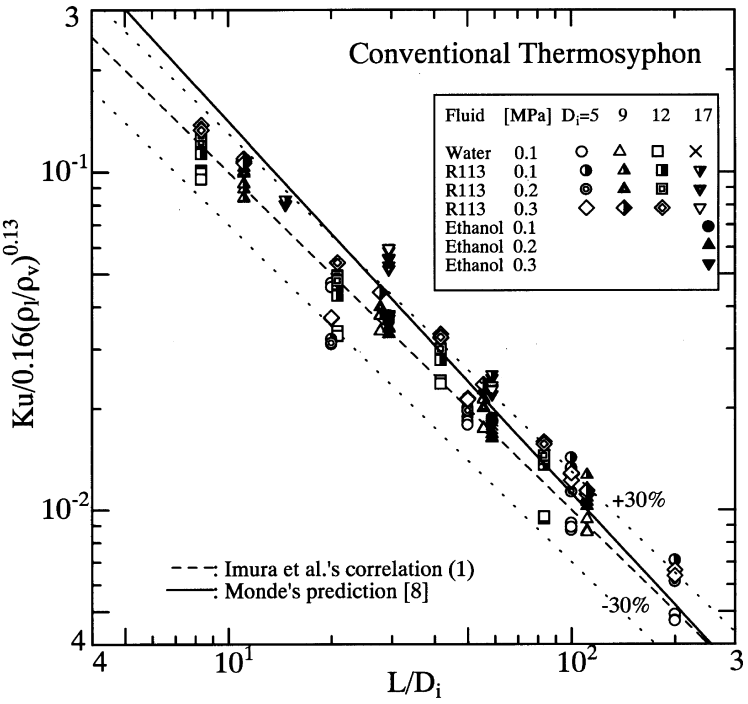

Fig. 6. CHF variation with length/diameter ratio of conventional thermosyphon.

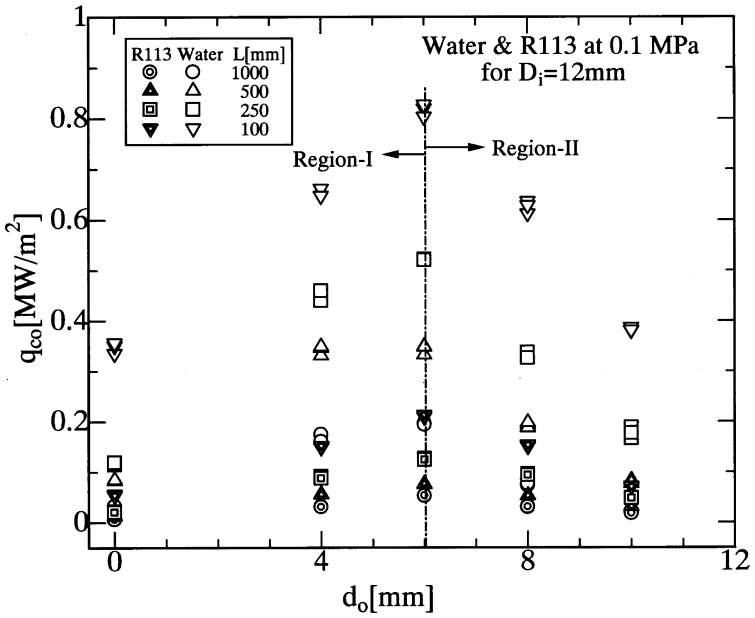

Fig. 7. CHF as a function of inner tube diameter.

diameter, but from the present experimental data, this effect is not clear.

3.6. *Enhancement of CHF due to inner tube*

Figure 8 (redrawn from Fig. 7 for convenience) shows the CHF enhancement as a function of inner tube diameter for a constant heated tube diameter, where length of the heated tube and working fluid are acting as parameters. Here, the CHF with inner tube, q_{co} is normalized by the CHF without inner tube, $q_{co,0}$ to denote the CHF enhancement. It is clear from Fig. 8 that for a constant inner tube diameter, the higher length of the heated tube gives the better CHF enhancement, while

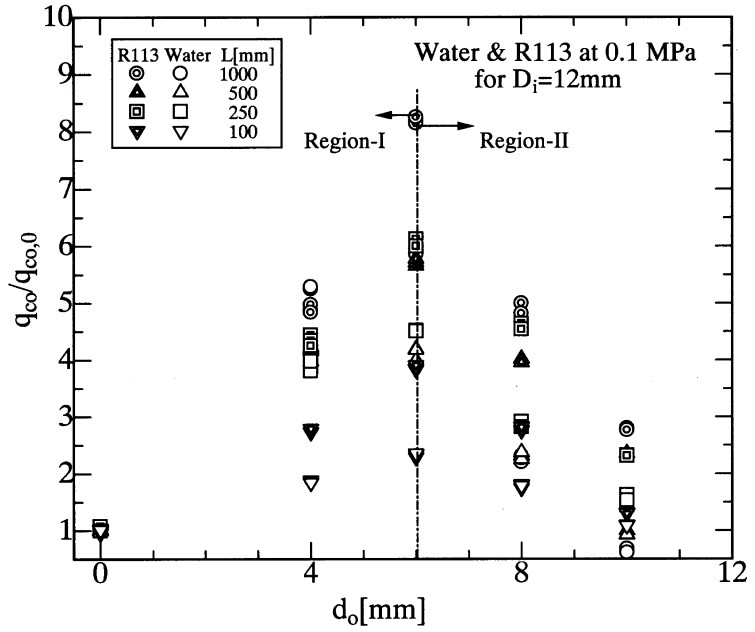

Fig. 8. CHF enhancement as a function of inner tube diameter.

R113 gives higher enhancement than water. The variation of the CHF enhancement with inner tube diameter is similar to the variation of the CHF as explained in the previous section. The enhancement of 8 for R113 and 6 for water are found for the thermosyphon of $L = 1000$ mm, $D_i = 12$ mm and $d_o = 6$ mm at atmospheric pressure.

3.7. *CHF characteristics*

It can be mentioned that the inner tube in a concentric-type thermosyphon enables some liquid to be supplied to the thermosyphon without any interaction with the escaping vapor flow and thus reduces the vapor–liquid interaction to some extent and consequently improves the CHF. Both the inside and outside diameters of the inner tube strongly affect the liquid flow through it and the vapor–liquid interactions in the annulus as shown in Fig. 3. So, depending upon the diameter of the inner tube, the CHF in a concentric-tube open thermosyphon can be categorized into two characteristic regions, I and II, as shown in Figs 7 and 8.

3.7.1. *Region I*

For the diameter of the inner tube smaller than the optimum value, the inner tube area is not large enough for the required liquid supply. By continuity, some liquid enters into the thermosyphon through the top of the annulus interacting with the escaping vapor as in a conventional single-tube thermosyphon. This vapor–liquid interaction can be reduced by increasing the inner tube diameter up to the optimum diameter, which in turn increases the amount of liquid to be supplied through the inner tube. Thus, the CHF increases in this region with the inner tube diameter as shown in Fig. 7. The CHF locations in this region are found at the upper half of the heated tube. The CHF mechanism in this region is closer to the conventional thermosyphon, as far as the vapor–liquid interaction in the annulus is concerned.

3.7.2. *Region II*

For the inner tube diameter larger than the optimum value, the inner tube area is large enough to supply the required amount of liquid to the annulus. The flow patterns at the open end of the thermosyphons in this region are as shown in the types of C, D, and E in Fig. 3 with increasing inner tube diameter. The CHF locations are found at the upper half of the heated tube except for the type E where the CHF is found to occur near the bottom of the heated tube as mentioned in section 3.3. Thus the CHF mechanism may be comparable to that in the natural convective boiling (NCB) in a vertical circular annulus where the outer tube is heated.

4. CHF correlations

As the CHF data in concentric-tube thermosyphon have been categorized into two characteristic regions, the independent governing parameters in each region are identified and correlations for predicting the CHF data are proposed accordingly.

4.1. *CHF correlation in Region I*

The improvement in the CHF would be achieved in Region I by some amount of liquid supplied through the inner tube. The inherent characteristics of the CHF are mentioned in section 3.7. The CHF data in this region can be correlated with the help of correlation (1) finding a suitable independent governing parameter accounting for the inner tube. Accordingly, the non-dimensional CHF, Φ^*, has been chosen from correlation (1) and the ratio of the frictional area in the inner tube to that in the annulus, $d_i/(D_i+d_o)$, is chosen as the governing parameter. Figure 9 shows the variation of Φ^* as a function of the parameter, $d_i/(D_i+d_o)$, where different symbols indicate the CHF data for a particular combination of the length and diameter of the outer tube. It is clear from Fig. 9 that Φ^* varies linearly with the parameter $d_i/(D_i+d_o)$ for a specific length of the outer tube within the experimental uncertainty. Different lines in Fig. 9 are obtained by the best fit of the experimental data for different lengths of the thermosyphon such that

$$\Phi^* = 4[1 + C(d_i/(D_i+d_o))] \tag{2}$$

which becomes the correlation (1) for the conventional thermosyphon without inner tube namely, d_o, $d_i = 0$. The slope varies according to the length of the thermosyphon and the working fluid as well. Thus the values of C can be approximated within $\pm 20\%$ by the equation (3).

$$C = 0.803[L/\sqrt{\sigma/g(\rho_l-\rho_v)}]^{0.5} \tag{3}$$

All the CHF data for water, ethanol and R113 belonging to Region I are plotted against $C(d_i/(D_i+d_o))$ in Fig. 10, and it is found that the CHF data can be predicted by equation (2) within $\pm 30\%$ except for very few cases where the experimental uncertainty is large. The statistical deviations of the CHF data predicted by equation (2) in comparison with the experimental data are shown in Table 3 which also exhibits the same for predicting the CHF in Region II, as discussed in the following section.

4.2. *CHF correlation in Region II*

The CHF in Region II seems to take place under a natural circulation flow through annular tube as mentioned in section 3.7. Monde et al. [13] pointed out that the equivalent heated diameter, D_{he} plays an important role in evaluating the CHF for natural convective boiling in annular tube and then proposed the CHF correlation as:

$$Ku = 0.16/[1 + 0.075(L/D_{he})] \tag{4}$$

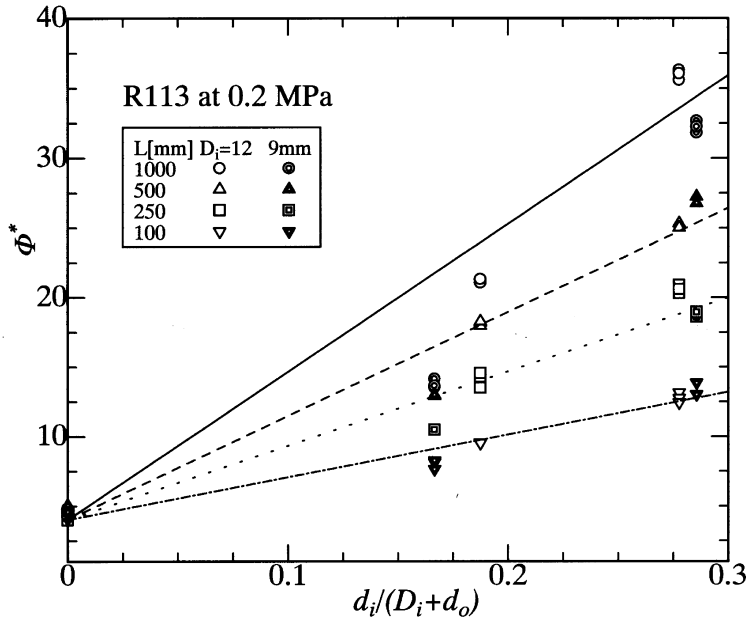

Fig. 9. Non-dimensional CHF, Φ*, as a function of $d_i/(D_i+d_o)$.

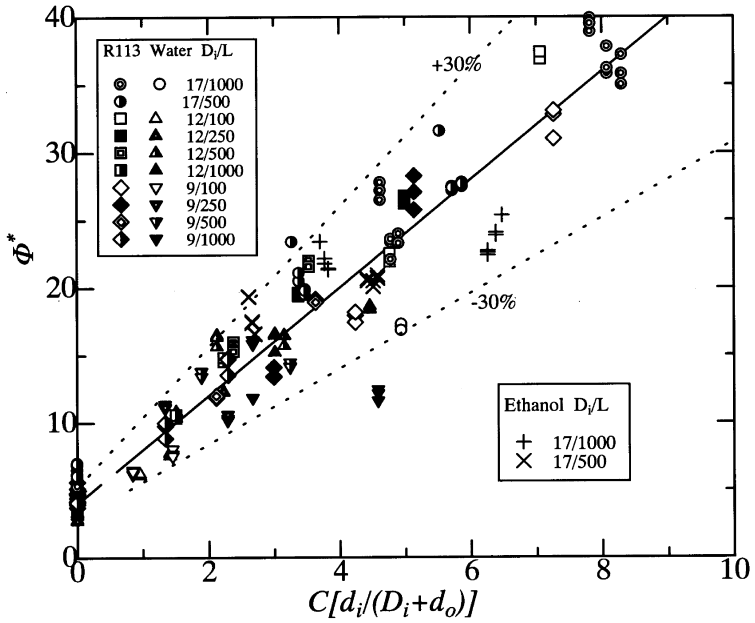

Fig. 10. CHF correlation in Region I.

for the NCB in vertical annuli of gaps ranging from 0.4–4 mm, where the inner tube is heated. Although the flow pattern in the concentric-tube thermosyphon becomes complicated compared with that in the natural convecting flow, we may plot the CHF data using reciprocal of the Kutateladze number, $1/Ku$ and L/D_{he} in the light of equation (4).

Figures 11, 12, and 13 show $1/Ku$ against L/D_{he} for water, ethanol and R113, respectively. The solid line in Figs 11, 12, and 13 denotes equation (4). It is clear from

Table 3. Errors of the CHF prediction

	Region I by equation (2)				Region II by equation (4)			
Fluid	*N*	E1	E2	E3	*N*	E1	E2	E3
Ethanol	18	0.025	0.121	0.143	17	0.149	0.174	0.207
R113	90	0.030	0.158	0.215	91	0.263	0.285	0.318
Water	26	−0.117	0.163	0.232	23*	−0.121	0.225	0.301
Total	134	0.001	0.154	0.211	131	0.180	0.260	0.302

*N (referred data) excluding anomalous data.
Average error: $E1 = \Sigma(1-q_{cal}/q_{exp})/N$.
Mean deviation: $E2 = \Sigma|1-q_{cal}/q_{exp}|/N$.
Standard deviation: $E3 = \sqrt{\Sigma(1-q_{cal}/q_{exp})^2/N}$.

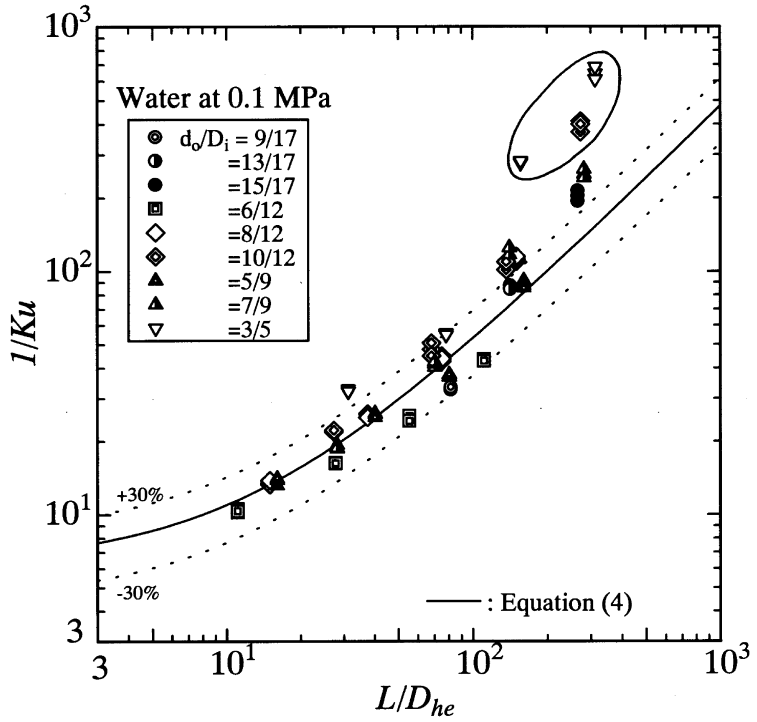

Fig. 11. CHF correlation in Region II for water.

Figs 11 and 12 that equation (4) predicts the CHF data in Region II well for the cases of ethanol and water except for a few cases (marked in Fig. 11) where annular gaps are smallest only for 1000 mm long outer tubes. The reason that the CHF data of $L = 1000$ mm and $s = 1$ mm for water become smaller than that of equation (4), is not clear.

For R113, the CHF data deviate from equation (4) as shown in Fig. 13. From the following reason, it may be of interest to compare these CHF data with correlation (5) of Monde and Yamaji [14] developed for the CHF in a vertical uniformly heated tube whose diameter is the same as the equivalent heated diameter, D_{he} for the annuli in Region II.

$$Ku = 0.16/[1+0.025(L/D_{he})] \quad (5)$$

Considering D_{he} in equations (4) and (5), one can notice that it shows different characters depending on whether inner or outer tube is heated in a two-tube system.

For the case of the inner tube heated, D_{he} becomes as:

$$D_{he} = d_o[(D_i/d_o)^2 - 1]$$

and for the other case,

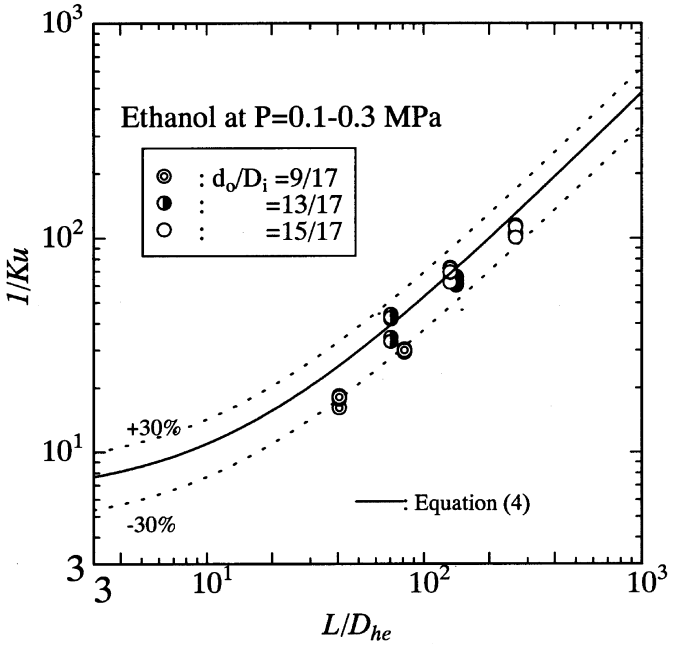

Fig. 12. CHF correlation in Region II for ethanol.

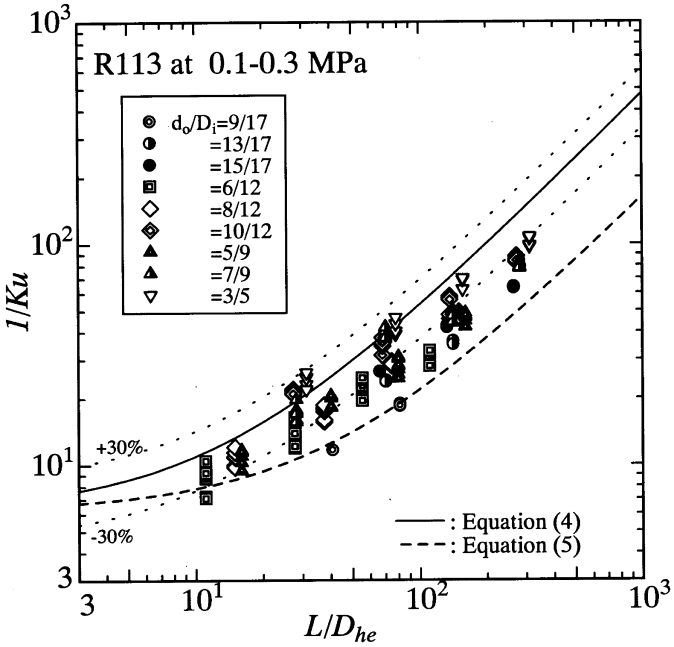

Fig. 13. CHF correlation in Region II for R113.

$$D_{he} = (d_o^2/D_i)[(D_i/d_o)^2 - 1]$$

The inner tube diameter, d_o, approaching to D_i gives the same narrow configuration for both cases. On the other hand, d_o being close to zero, gives different configurations. For the inner tube heated, this limiting condition corresponds to the vertical heated condition in pool boiling, while for the outer tube heated it corresponds to the NCB in a single tube where the CHF can be predicted by equation (5). Therefore, the reason why the CHF data for R113 shift from equation (4) to equation (5) may be due to the role of equivalent heated diameter, D_{he}. In order to determine the effect of D_{he}, one needs to have the CHF data for different liquid having smaller density ratio, which is being done at present.

4.3. *Boundary between Regions I and II*

The flow situation of liquid and vapor at the boundary between Regions I and II is similar to that of the type C in Fig. 3. The CHF at this boundary is believed to occur by the vigorous boiling with least vapor–liquid interactions in the annulus resulting in dryout of the heated wall near the top. This boundary tentatively corresponds to the optimum diameter of the inner tube which can be calculated from the intersection of the correlations for Regions I and II. It is worth mentioning that this boundary is very important from the engineering point of view as engineers would look for this point in designing a proper heat transfer device. Further study is necessary for predicting this boundary.

5. Conclusions

An experimental study of the CHF characteristics in a concentric-tube open thermosyphon has been presented. The main findings are as follows:

(1) For a particular heated tube diameter working with a specific fluid, there is an optimum diameter of the inner tube at which the CHF is maximum.
(2) The optimum diameter of the inner tube divides the CHF into two characteristic regions. The CHF in Region I appears to be comparable to conventional thermosyphon and the CHF in Region II seems to be similar to that in a natural convective boiling in vertical circular annuli.
(3) The CHF data in Region I can be predicted by the following equation within $\pm 30\%$

$$\frac{4L}{D_i}\frac{q_{co}/\rho_v H_{fg}}{4\sqrt{\sigma(\rho_l-\rho_v)g/\rho_v^2}} = 0.64\left[\frac{\rho_l}{\rho_v}\right]^{0.13} \times \left[1+0.803\{L/\sqrt{\sigma/g(\rho_l-\rho_v)}\}^{0.5}\left\{\frac{d_i}{D_i+d_o}\right\}\right]$$

(4) The CHF data in Region II can be predicted by equation (4) within $\pm 30\%$, except for that of R113.

Acknowledgement

The authors gratefully acknowledge the contributions of Mr T. Moritomo, Mr T. Furutake, Mr M. Murashige and Mr K. Nakashima in building the experimental setup and collecting data.

References

[1] Tien CL, Chung KS. Entrainment limits in heat pipes. AIAA J 1979;17:643–6.
[2] Smirnov Ye L. Critical heat flux in flooding in vertical channels. Heat Transfer—Soviet Research 1984;16–3:19–23.
[3] Imura H, Sasaguchi K, Kozai H, Numata S. Critical heat flux in a closed two-phase thermosyphon. Int J Heat Mass Transfer 1983;26:1181–8.
[4] Dobran F. Steady-state characteristics and stability thresholds of a closed two-phase thermosyphon. Int J Heat Mass Transfer 1985;26:949–57.
[5] Reed JC, Tien CL. Modeling of a two-phase closed thermosyphon. Trans ASME J Heat Transfer 1987;109:720–30.
[6] Lock GSH. On the flooding limit in evaporative, tubular thermosyphon. Int Commun Heat Mass Transfer 1993;20:422–8.
[7] Katto Y. Limit conditions of steady-state countercurrent annular flow and the onset of flooding, with reference to the CHF of boiling in a bottom-closed vertical tube. Int J Multiphase Flow 1994;20(1):45–61.
[8] Monde M. Analytical study of critical heat flux in two-phase thermosyphon: relationship between maximum falling liquid rate and critical heat flux. Trans ASME J Heat Transfer 1996;118:422–8.
[9] Seki N, Fukusako S, Koguchi K. Single-phase heat transfer characteristics of concentric-tube thermosyphon. Wärme- und Stoffübertragung 1980;14:189–99.
[10] Seki N, Fukusako S, Koguchi K. An experimental investigation of boiling heat transfer of fluorocarbon R-11 refrigerant for concentric-tube thermosyphon. Trans ASME J Heat Transfer 1981;103:472–7.
[11] Fukuda T, Kondoh T, Hasegawa S. Thermal characteristics of double cylinder closed thermosyphon. Proc 1st KSME–JSME Thermal Fluids Eng Conf, Vol. 1, 1988, pp. 253–8.
[12] Mitsutake Y, Monde M, Hasan MZ. Experimental study of the critical heat flux in open concentric-tube thermosyphon. Proc 3rd KSME–JSME Thermal Engineering Conference (Kyongju), Vol. 1, 1996, pp. 71–6.
[13] Monde M, Mitsutake Y, Kubo S. Critical heat flux during natural convective boiling on uniformly heated inner tubes

in vertical annular tubes submerged in saturated liquid. Wärme- und Stoffübertragung 1994;29:271–6.
[14] Monde M, Yamaji K. Critical heat flux during natural convective boiling in a vertical uniformly heated tubes submerged in saturated liquid. Proc 9th Heat Transfer Conf, Vol. 2, 1990, pp. 111–6.
[15] Rohsenow WM. A method of correlating of heat transfer data for surface boiling of liquids. Trans ASME J Heat Transfer 1962;84:969.
[16] Imura H, Kusuda H, Ogata J, Miyazaki T. Heat transfer in two-phase closed-type thermosyphon. Heat Transfer—Japanese Research 1979;8(2):41–53.
[17] Collier JG. Convective boiling and condensation. 2nd ed., McGraw-Hill Inc., 1981, Chap. 7, p. 208.